Band Alignment in Quantum Wells from Automatically Tuned DFT+U

Kolesov, G.; Lin, C.; Kojima, K.; Knyazev, A.; Katz, J.

Abstract

Band alignment between two materials is of fundamental importance for multitude of applications. However, density functional theory (DFT) either underestimates the bandgap - as is the case with local density approximation (LDA) or generalized gradient approximation (GGA) - or is highly computationally demanding, as is the case with hybrid-functional methods. The latter can become prohibitive in electronic-structure calculations of supercells which describe quantum wells. We propose to apply the DFT+U method, with U for each atomic shell being treated as set of tuning parameters, to automatically fit the bulk bandgap and the lattice constant, and then use thus obtained U parameters in large supercell calculations to determine the band alignment. We apply this procedure to InP/In0.5Ga0.5As, In0.5Ga0.5As/In0.5Al0.5As and InP/In0.5Al0.5As quantum wells, and obtain good agreement with experimental results. Although this procedure requires some experimental input, it provides both meaningful valence and conduction band offsets while,crucially, lattice relaxation is taken into account. The computational cost of this procedure is comparable to that of LDA. We believe that this is a practical procedure that can be useful for providing accurate estimate of band alignments between more complicated alloys.

Band Alignment in Quantum Wells from Automatically Tuned DFT+U

Grigory Kolesov[1,2][*][‡], Chungwei Lin[1][†][‡], Andrew Knyazev[1], Keisuke Kojima[1], Joseph Katz[1],

Koichi Akiyama[3], Eiji Nakai[4], Hiroyuki Kawahara[4]

[1]*Mitsubishi Electric Research Laboratories,*

201 Broadway, Cambridge, MA 02139, USA

[2]*Harvard University, Cambridge, MA 02138, USA*

[3]*Mitsubishi Electric Corporation, 8-1-1,*

Tsukaguchi Honmachi, Amagasaki, Hyogo, Japan, 661-8661

[4]*Mitsubishi Electric Corporation, 4-1,*

Mizuhara, Itami, Hyogo, Japan, 664-8641

(Dated: April 10, 2019)

---

[*] email: gkolesov@seas.harvard.edu

[†] email: clin@merl.com

[‡] These authors contributed equally.

Abstract

Band alignment between two materials is of fundamental importance for multitude of applications. However, density functional theory (DFT) either underestimates the bandgap - as is the case with local density approximation (LDA) or generalized gradient approximation (GGA) - or is highly computationally demanding, as is the case with hybrid-functional methods. The latter can become prohibitive in electronic-structure calculations of supercells which describe quantum wells. We propose to apply the DFT+U method, with U for each atomic shell being treated as set of tuning parameters, to automatically fit the bulk bandgap *and* the lattice constant, and then use thus obtained U parameters in large supercell calculations to determine the band alignment. We apply this procedure to InP/In$_{0.5}$Ga$_{0.5}$As, In$_{0.5}$Ga$_{0.5}$As/In$_{0.5}$Al$_{0.5}$As and InP/In$_{0.5}$Al$_{0.5}$As quantum wells, and obtain good agreement with experimental results. Although this procedure requires some experimental input, it provides both meaningful valence and conduction band offsets while, crucially, lattice relaxation is taken into account. The computational cost of this procedure is comparable to that of LDA. We believe that this is a practical procedure that can be useful for providing accurate estimate of band alignments between more complicated alloys.

I. INTRODUCTION

Band alignment between two materials is crucial for many industrial applications, such as light-emitting diodes and diode lasers[1], field-effect transistors[2], photovoltaics[3], photocatalysts[4], photon waveguides[5] and others. The most common theoretical approach used to determine the band alignment is density functional theory (DFT)[6], which is usually adequate for qualitatively comparing different materials, but is unsatisfactory quantitatively. One serious difficulty of DFT is that it underestimates the bandgap when using standard local density approximation (LDA) or generalized gradient approximation (GGA) exchange-correlation functionals. When using GGA or LDA to determine the band alignment, only the valence band offset (VBO) can be directly determined by the calculation with acceptable accuracy; the conduction band offset (CBO) is inferred from the experimental bandgap of the bulk materials[7–10]. Using this approach, the CBO cannot be determined when the interface strain changes the bandgap of a material. The precision of a bulk bandgap can be greatly improved by using better approximations, such as the many-body GW approach[11,12] or hybrid-functional DFT[13,14]. These calculations, however, require significantly more computational resources than those required for LDA or GGA, so that supercell calculations to determine the band alignment can become too time consuming, and supercell relaxation is often out of reach. DFT+U is a method where the exchange-correlation functional is corrected by a set of U values which are applied to selected atomic orbitals[15,16]. DFT+U allows adjustment of the bulk bandgap to the experimental value by using U values as tuning parameters. This approach was explored, for example, in Ref.[10] with application to the band-alignment problem. The results are not satisfactory in that DFT+U, while making bandgap-fitting possible for a fixed lattice structure, does not reproduce the proper structure of the material when the structure is allowed to relax. The same authors also proposed a different empirical approach using the non-local external potential[17] which provides the orbital-dependent energy shift to correct the bandgap. Another promising approach is the use of meta-GGA functionals such as the modified Becke-Johnson functionals[18–21], which are computationally inexpensive, but provide better estimation of the bandgap. While *ab initio* methods such as GW, hybrid-functional and meta-GGA DFT offer significant improvements over LDA/GGA-functional DFT they are still quite problematic to use in practical calculations: GW is accurate only in its self-consistent realization[22,23] for some materials and less

accurate for others[24,25]; the computational cost of this method is prohibitive in supercell and lattice relaxation calculations. Both hybrid-functional and meta-GGA DFT require tuning of the parameters of the functional (e.g. screening length and fraction of exchange) to the material to achieve sufficient accuracy[26–28], while large supercells and lattice relaxation are still difficult with the former.

In this paper, we re-examine DFT+U as a practical "black-box" method for the determination of the band alignment between two semiconductors. The U values of the bulk material are determined completely automatically by an optimization procedure which adjusts them until the calculation reproduces i) the experimental bandgap *and* ii) the lattice parameters. The same U values are then used in the superlattice calculations. This procedure is semi-empirical, in the sense that some experimental inputs are needed. However, it takes the interface strain into account and results in accurate VBO and CBO, while using minimalistic basis sets and computational resources comparable to those required by LDA or GGA functionals. This method thus allows us to use supercells containing 320 atoms to determine the band alignment (see Fig. 1). We apply this procedure to $In_{0.5}Ga_{0.5}As/InP$ (denoted as InGaAs/InP below) and $In_{0.5}Ga_{0.5}As/In_{0.5}Al_{0.5}As$ (InGaAs/InAlAs) superlattices, with varying InGaAs widths. All alloys studied here are lattice-matched to InP. The change of the band alignment is quantitatively consistent with the reported experiments, and bandgaps of the full superlattice are consistent with photo-luminescent (PL) measurements. The same procedure is applied to InP/InAlAs to test transitivity[29]. The rest of the paper is organized as follows. In Section II we describe the procedure to determine the band alignment, including a summary of bulk experimental values. In Section III we show our results for InP/InGaAs, InGaAs/InAlAs, and InP/InAlAs lattice calculations. The comparison to the photo-luminescent measurements is shown and discussed. A brief conclusion is given in Section IV.

II. METHOD

A. Computational details

In the main part of this work we used the SIESTA package[30]. The pseudopotential input files were downloaded from the SIESTA website. In and Ga pseudopotentials were generated

with $4d$ (In) and $3d$ (Ga) electrons included in the valence. We used single-ζ + polarization shell (SZP) basis sets, which were optimized in a bulk setup (such as GaAs or InP) using the Optimizer tool from the SIESTA package[31] with basis pressure equal to 0.2 GPa and the Perdew-Burke-Ernzerhof (PBE) DFT functional[32]. The optimized SZP basis sets have been shown to have similar quality to a generic double-ζ + polarization (DZP) basis[31]. The spin-orbit coupling was not included in the calculations. This is done in order to reduce the computational cost and in order to avoid convergence difficulties while probing different sets of U parameters. Thus we attempt to capture the essential features of the quantum wells, that is band alignment in the relaxed structures, with U parameters only. All geometry relaxations were performed using the conjugate gradient method.

For the bulk calculation we used conventional unit cells and $7 \times 7 \times 7$ Monkhorst-Pack k-point sampling. All materials considered in this work have zincblende structures. For alloy materials such as InGaAs we also used the conventional unit cell. The same unit cells were replicated to construct the interface supercells. We did not use virtual crystal approximation (VCA) or coherent potential approximation (CPA)[7,8] in this work.

DFT+U[15,16,33] is a method which is in principle close to the hybrid-functional approach in that it attempts to address the electron-electron interaction problem of local DFT functionals[34,35]. In the DFT+U approach an atomic orbital-dependent U correction is added to the DFT Hamiltonian[15]. In the Dudarev spherically averaged approach[16], which was employed here, this results in an effective orbital-dependent potential:

$$V_{jk}^{\text{LDA}+U} = V_{jk}^{\text{LDA}} + U \left[\frac{1}{2}\delta_{jk} - \rho_{jk} \right],$$ (1)

where j, k are orbital indices and ρ is the electronic single-particle density matrix. The parameter U for each orbital can in principle be computed *ab initio*[34–37] but in practice is often fitted to reproduce experimental results such as the bandgap. Eq. (1) shows that for positive U the energy levels are shifted up for unoccupied orbitals and down for occupied ones.

B. U optimization

In this work we used the DFT+U approach where U values were fitted in a systematic way. Given a bulk crystal structure we enable U for each valence atomic orbital, except

for semicore orbitals such as $4d$ in In, which are completely filled and lie very deeply in the valence band of the materials we study here. We then apply the simplex method as implemented in the Optimizer tool from the SIESTA package to minimize an objective function:

$$f\left(\mathbf{U}\right) = w_g \left[E_g\left(\mathbf{U}\right) - E_g^{\text{exp}}\right]^2 + w_a \sum_{i=1}^{3} \left[\mathbf{a}_i(\mathbf{U}) - \mathbf{a}_i^{\text{exp}}\right]^2. \tag{2}$$

Here $\mathbf{U}$ denotes set of all values of U_j, j being a combined index for an atomic species, principal and angular momentum quantum numbers; E_g and $\mathbf{a}_i$ denote bandgap and lattice vectors respectively; superscript "exp" denotes experimental values. w_g and w_a are weights, which we chose to be 0.33 eV^{-2} and 0.67 Å^{-2}. For a given $\mathbf{U}$, the full lattice relaxation followed by a bandgap computation is performed.

We would like to make a few remarks. i) The minimization is deemed sufficient when $f(\mathbf{U}) \lesssim 10^{-3}$ because of experimental uncertainties. ii) Here $\mathbf{U}$ are treated as free parameters, which are not only aimed at correcting deficiencies of the PBE functional but also serve as a finite basis set correction[38]. Thus U's could in principle be negative, although in this work we restrict them to be positive. iii) The optimization is performed on the bulk unit cell and is computationally inexpensive, typically taking several hours on four CPU cores. We point out that it is to satisfy both constraints that complicates the optimization; to fit only the band gap is actually quite easy.

C. Theoretical motivation

Here we provide the theoretical motivation on why fitting the bulk lattice constant *and* band structure can give a correct band alignment. For the general Hamiltonian

$$H = T + v_{ext} + V_{e-e}, \tag{3}$$

where T represents the kinetic energy, v_{ext} the external potential (depending on positions of ions), V_{e-e} the Coulomb electron-electron interaction, Hohenberg-Kohn theorem[39] establishes a one-to-one relationship between $v_{ext}(\mathbf{r})$ and the many-body ground-state density $n(\mathbf{r})$ – a given $n(\mathbf{r})$ gives a unique $v_{ext}(\mathbf{r})$ and vice versa, i.e.,

$$v_{ext}(\mathbf{r}) \Leftrightarrow n(\mathbf{r}) \tag{4}$$

Therefore for a ground-state wave function $|\Psi[v_{ext}(\mathbf{r})]\rangle$ that corresponds to an external potential $v_{ext}(\mathbf{r})$, we can denote the *same* wave function as $|\Psi[v_{ext}(\mathbf{r})]\rangle = |\Psi[n(\mathbf{r})]\rangle$. For a *given* external potential $\tilde{v}_{ext}(\mathbf{r})$, one defines the density functional that maps a charge density $n(\mathbf{r})$ to an expectation value of total energy:

$$E[n(\mathbf{r}); \tilde{v}_{ext}(\mathbf{r})] \equiv \langle \Psi[n(\mathbf{r})]|T + \tilde{v}_{ext} + V_{e-e}|\Psi[n(\mathbf{r})]\rangle. \tag{5}$$

By the variational principle, the energy expectation value is at its global minimum when the wave function is the ground state of $H = T + \tilde{v}_{ext} + V_{e-e}$, which has a ground-state density $\tilde{n}(\mathbf{r})$. Consequently, the density functional $E[n(\mathbf{r}); \tilde{v}_{ext}(\mathbf{r})]$ has the global minimum when $n(\mathbf{r}) = \tilde{n}(\mathbf{r})$, with the value of ground-state energy. Functionals of kinetic energy $\langle \Psi[n(\mathbf{r})]|T|\Psi[n(\mathbf{r})]\rangle$ and Coulomb energy $\langle \Psi[n(\mathbf{r})]|V_{e-e}|\Psi[n(\mathbf{r})]\rangle$ are universal, but their exact functional forms are not known.

A well approximated density functional is supposed to give experimental results. There are two immediate consequences for the exact density functional: (i) $E[n(\mathbf{r}); v_{ext}(\mathbf{r})]$ is at the minimum when $v_{ext}(\mathbf{r})$ represents the observed lattice structure; (ii) the resulting charge density $n(\mathbf{r})$ is identical to the real charge density. These conditions can be seen as one and formally justified through the use of the multi-component DFT[40], where $E[n(\mathbf{r}), \Gamma(\mathbf{R})]$, a functional of both electron and nuclear densities $n(\mathbf{r})$ and $\Gamma(\mathbf{R})$, is minimized. Motivated by these two conditions, we proposed that a parameterized functional should simultaneously fit the observed lattice structure [condition (i)] and the measured band gap [condition (ii)]. The measured band gap serves as a measure of charge distribution between ions. We regard a parameterized functional that satisfies these two conditions as a good functional for a given material, and propose to use LDA+U, with U's being parameters tuned to meet these two conditions, to obtain the material-specific good functional. We expect that the correct functional will provide the correct band alignment between two bulk materials. As we will demonstrate, this procedure is indeed found to be quantitatively useful for determining the band alignments.

In addition to correcting exchange-correlation functional, $+U$ method can be used outside of the density functional theory as a way of reducing basis-set superposition error. For example, Kulik and co-workers applied $+U$ method in Hartree-Fock calculations with a minimalistic basis set[38]. In this work we also use minimalistic basis sets and thus our optimization procedure can take advantage of this application of the $+U$ method.

As shown below, the values of U obtainend with our optimization procedure are found to be significantly large only for the p orbitals. This is not surprising, since recent direct calculations[37] of U have shown that in transition-metal oxides, contrary to what was assumed before, U on p-orbitals of the oxygen atoms exceed or on the order of U calculated for the d-orbitals of the transition metal atom.

D. Determination of the band alignment

We consider band alignments between InGaAs and InP, and between InGaAs and InAlAs. In both cases InGaAs is the "well" material which has a bandgap of 0.76 eV; InP and InAlAs serve as the "barrier" materials whose bandgaps are around 1.4 eV. All three materials have lattice constants of 5.86Å, lattice matched to InP. The band diagram of a quantum well or a superlattice is illustrated in Fig. 2(a).

To determine the band alignment, superlattices of $(\text{InGaAs})_n/(\text{InP})_{20}$, $(\text{InGaAs})_n/(\text{InAlAs})_{20}$, and $(\text{InAlAs})_{20}/(\text{InP})_{20}$ are used, with the conventional zincblende unit cell serving as the basic building block. As illustrated in Fig. 2(a), the supercell has a period of $1 \times 1 \times (20 + n)$, with the stacking direction defined as z. Because all three materials have almost the same lattice constant which is reproduced in our bulk calculations with optimized U parameters, we fix the in-plane lattice constant to that of bulk InP and allow only relaxation of the supercell in the z-direction and relaxation of the ionic positions in our calculations. As the projected density of states (DOS) recovers its bulk profile away from the interface, the band alignment is determined by the projected DOS in the middle of InGaAs, InP, and InAlAs respectively.

E. Summary of bulk experiments

We conclude this section by summarizing the experimental results of two classes of III-V zincblende alloys. The first class is $\text{Ga}_x\text{In}_{1-x}\text{As}_y\text{P}_{1-y}$, whose lattice constant is given by[41,42]

$$a_{\text{GaInAsP}}(x, y) = 5.8696 - 0.4184x + 0.1894y + 0.0130xy. \tag{6}$$

The bulk bandgaps are[42]

$$E_{\text{GaInAsP}}(x, y) = 1.35 + 0.668x - 1.17y + 0.758x^2 + 0.18y^2 - 0.069xy - 0.322x^2y + 0.03xy^2 \tag{7}$$

Eq. (6) and (7) are room-temperature results. When lowering the temperature, the bandgap becomes larger and the lattice constant smaller. For example, InP at 4K has a bandgap around 1.45 eV and a lattice constant around 5.85Å.

The second class of alloys is $In_{1-x-y}Ga_xAl_yAs$. The physical quantities can be parametrized as[43]

$$P(In_{1-x-y}Ga_xAl_yAs) = P(InAs)(1 - x - y) + P(GaAs)x + P(AlAs)y \qquad (8)$$

Using the bulk data summarized in Ref.[44], the lattice constants of GaAs, GaP, InAs, and AlAs are respectively 5.6533Å, 5.4505Å, 6.0584Å, and 5.660Å. The lattice constant of this class of alloys is therefore parameterized as

$$a_{InGaAlAs}(x, y) = 6.0584(1 - x - y) + 5.6533x + 5.660y$$
$$= 6.0584 - 0.4051x - 0.3984y. \qquad (9)$$

The bulk bandgap is obtained from

$$E_{InGaAlAs}(In_{1-x-y}Ga_xAl_yAs) = 0.36 + 2.093y + 0.629x + 0.577y^2$$
$$+ 0.436x^2 + 1.013xy - 2.0xy(1 - x - y)eV. \qquad (10)$$

For alloys that are lattice matched to InP (5.86 Å) where $x + y = 0.47$, i.e., $In_{0.53}Ga_{0.47-y}Al_yAs$, the bandgap fitted from Ref.[45]

$$E(y) = 0.76 \pm 0.04 + (1.04 \pm 0.10)y + (0.87 \pm 0.13)y^2. \qquad (11)$$

Directly using Eq. (10), we get $E(y) = 0.7519 + 1.0321y + 1.06y^2$. It appears that the coefficient of y^2 is not consistent between these two expressions. However since $y < 0.47$, the error is at most $(1.06 - 0.87) \times 0.47^2 = 0.042$ eV, which sets the uncertainty in our calculations. The experimental results summarized here are used to optimize the U values in the DFT+U functional.

III. RESULTS

A. Optimized U values

The U values for InP, InGaAs, and InAlAs are given in Table I. As described in Section II B, these U values are computationally optimized to fit both experimental bulk lattice

Material	$E_g - E_g^{\mathrm{exp}}$ (eV)	$a - a^{\mathrm{exp}}$ (Å)	Species	n quantum number	U_s (eV)	U_p (eV)
$\mathrm{In_{0.5}Ga_{0.5}As}$	-0.03 (0.76)	-0.01 (5.87)	In	5	0.00	7.58
			Ga	4	0.00	3.66
			As	4	0.02	0.20
InP	-0.03 (1.34)	-0.02 (5.87)	In	5	0.00	4.23
			P	3	0.00	0.48
$\mathrm{In_{0.5}Al_{0.5}As}$	0.00 (1.47)	0.00 (5.87)	In	5	0.01	3.31
			Al	3	0.41	2.80
			As	4	0.03	0.15

TABLE I: U parameters optimized for best fit to experimental values of bandgap (E_g) and lattice constant (a) (Section II B). U_s denotes the value of U applied to the s-shell of the corresponding atom, while U_p denotes U values applied to p-shells. With the values of U presented here all angles are 90° in the optimized conventional unit cells. In column 2 and 3 the experimental values are indicated in parentheses.

structure and bandgap. It can be seen that U values of the same species strongly depend on the material. For example for the $5p$-shell of the In atom, the value of U_p is 7.58, 4.23 and 3.31 eV in InGaAs, InP and InAlAs respectively. This is expected, because the value of U incorporates screening effects[15] and thus depends on the environment of the atom.

There are two other trends clearly visible in Table I. First, the values U_s for all species are small or nearly zero. Second, the U values for anionic atoms are much smaller then U for cationic atoms. This indicates that both the optimization of the geometry and the bandgap is largely controlled by p-states of the cationic atoms, which constitute the largest part of the conduction band and a smaller but not insignificant part of the valence band.

B. Bulk band offsets in InGaAs/InP, InGaAs/InAlAs, and InAlAs/InP

To test our procedure we first study band offsets in bulk heterostructures. For each combination of materials we construct 20/20 supercell, that is a supercell that has total 40 conventional unit cells in z-direction (20 for each material) and 1 unit cell in x- and y-directions (see, for example, Fig. 2(a) with $n = 20$). We used $3 \times 3 \times 1$ k-point sampling

(a) InGaAs/InP

(b) InGaAs/InAlAs
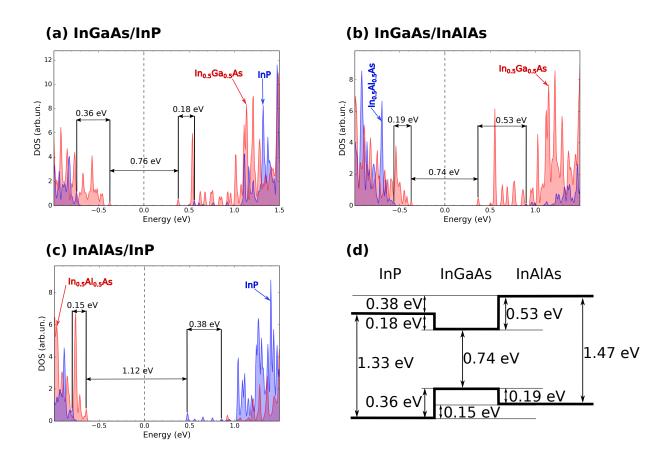
(c) InAlAs/InP

(d)

FIG. 1: (a) Projected DOS for $(InGaAs)_{20}/(InP)_{20}$. (b) Projected DOS for $(InGaAs)_{20}/(InP)_{20}$. (c) Projected DOS for $(InGaAs)_{20}/(InP)_{20}$. The intervals show, from left to right, VBO, bandgap and CBO. (d) The combined band diagram InP/InGaAs/InAlAs. The VBO's and CBO's of different interfaces satisfy the transitivity rule within $\lesssim 0.05$ eV. The bulk band gaps are derived from the bulk calculation for each material.

during the initial geometry optimization and $7 \times 7 \times 1$ for the final geometry optimization and PDOS calculation. During the geometry optimization 5 unit cell-thick layers in the middle of each material were kept rigid to preserve bulk lattice parameters.

The resulting PDOS for each combination of materials is presented in Fig. 1 (a)-(c).

For $(InGaAs)_20/(InP)_20$ (Fig. 1(a)) the computed VBO is 0.36 eV and CBO 0.18 eV. The experimental results for VBO agree well on 0.35 eV value which is in excellent agreement with our computed value[46]. The results for CBO seem to be less consistent and experiments report values in 0.2-0.4 eV range[46]. The CBO of 0.18 eV computed here is thus at the lower edge of this range.

For $(InGaAs)_20/(InAlAs)_20$ (Fig. 1(b)) the computed VBO is 0.19 eV and CBO 0.53 eV.

This is in excellent agreement with averaged experimental values for this heterojunction of 0.19 eV and 0.51 eV, respectively[46].

For $(InP)_{20}/(InAlAs)_{20}$ (Fig. 1(c)) the experimental values for VBO are reported to be in 0.11-0.31 eV range with 0.155 eV recommended by Vurgaftman et al[46]. Our computed values of 0.153 eV agrees with this recommendation. For CBO of this heterojuction the experimental data is scarce and CBO is reported to be $2.86\Delta E_g$ [47], which should result in $(1.47 - 1.34) \cdot 2.86 = 0.37$ eV agreeing with the 0.38 eV computed by us.

The composite diagram for all computed band gaps and offsets is shown on Fig.1(d). The VBOs and CBOs of all three materials are transitive within $\lesssim 0.05$ eV. This degree of non-transitivity agrees well with experiments[46], but here is most likely is a result of the computational uncertainty.

C. Bands offsets in InGaAs/InP and InGaAs/InAlAs quantum wells

Fig. 2(b)-(d) show the computed projected DOS for $(InGaAs)_n/(InP)_{20}$ with $n = 10, 8, 6$. The bandgap increases as the quantum well width, characterized by n, decreases due to the increasing quantum confinement. The computed bandgap is in good agreement with the PL experiments, as summarized in Table II.As expected, the band alignment also exhibits the effects of the quantum confinement: with the well width decreasing the well band gap expands and the VBO shrinks from 0.32 eV to 0.23 eV whereas CBO from 0.14 eV to 0.09 eV. Due to the confinement these band offsets are below the range of experimental values for bulk interfaces and bulk band offsets computed by us (Fig. 1(a)).

Fig. 3(b)-(d) show the computed projected DOS for $(InGaAs)_n/(InAlAs)_{20}$ with $n = 10, 8, 6$. The bandgap also opens up with decreasing n due to the stronger quantum confinement. The band alignment changes correspondingly with expanding band gap : the VBO shrinks from 0.20 eV to 0.15 eV whereas the CBO shrinks from 0.43 to 0.40 eV. We notice that again the band offset values in quantum wells are smaller than those in bulk, and this is consistent with the enlarged band gap caused by the quantum confinement.

As InP and InAlAs have similar bandgaps and lattice constants, our calculations show that InGaAs/InP has the larger VBO and the smaller CBO, whereas InGaAs/InAlAs has the larger CBO and the smaller VBO. This trend is consistent with the experiments. Generally, the VBO/CBO values depend only weakly on the quantum well width. The bandgap,

(a)

(b) 10 InGaAs/20 InP

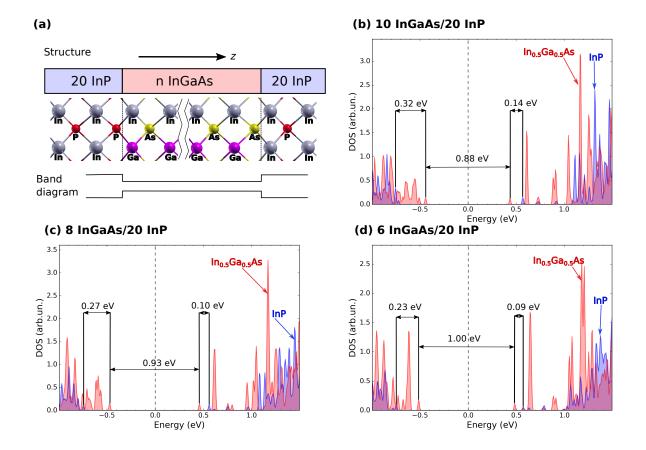**(c) 8 InGaAs/20 InP**

(d) 6 InGaAs/20 InP

FIG. 2: (a) Illustration of the structure and the band diagram of the superlattice used to determine the band alignment between InP and InGaAs. (b) Projected DOS for $(InGaAs)_{10}/(InP)_{20}$. (c) Projected DOS for $(InGaAs)_8/(InP)_{20}$. (d) Projected DOS for $(InGaAs)_6/(InP)_{20}$. The intervals show, from left to right, VBO, bandgap and CBO.

however, displays an observable dependence on quantum well width, and will be discussed in Section III D in terms of photoluminescent measurements.

D. Comparison to photoluminescent measurements

Quantum well	Bandgap (theory)	PL measurement	Experimental well width
6 InGaAs/20 InP	1.00 eV	0.94 eV	4nm
8 InGaAs/20 InP	0.93 eV	0.91 eV	5nm
10 InGaAs/20 InP	0.88 eV	0.89 eV	6nm

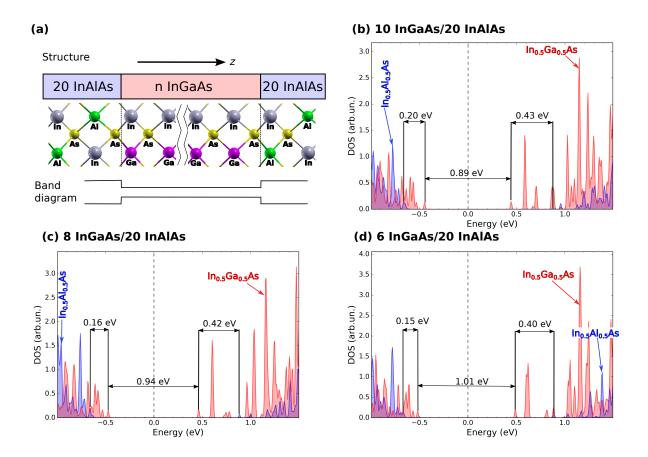TABLE II: The bandgap of InGaAs/InP, as a function of quantum well width.

FIG. 3: (a) Illustration of the superlattice structure used to determine the band alignment between InAlAs and InGaAs. (b) Projected DOS for $(InGaAs)_{10}/(InAlAs)_{10}$. (c) Projected DOS for $(InGaAs)_8/(InAlAs)_{10}$. (d) Projected DOS for $(InGaAs)_6/(InAlAs)_{10}$. The intervals show, from left to right, VBO, bandgap and CBO.

To further test the calculations, we prepared quantum wells of 4nm, 5nm and 6nm InGaAs as well as 30nm InP, and perform the PL measurements. The superlattice is grown using the standard MOCVD (Metal-Organic Chemical Vapour Deposition) method. The PL experiments were carried out at 300 K. The results are shown in Fig. 4. The Gaussian fits imply that the PL spectra display at least two peaks, which we interpret as the heavy hole and light hole splitting. The observed lowest-energy peak corresponds to the bandgap of the quantum well, and is summarized in Table II. As the lattice constant is 5.86 Å, InGaAs wells of width 4nm, 5nm, 6nm are close to 6, 8, 10 InGaAs unit cells. The computed bandgaps are also given in Table II, and good agreement is seen. Our simulation tends to somewhat overestimate the effect of the quantum confinement; this, at least in part, is due to the well widths used in $(InGaAs)_6/$ and $(InGaAs)_8/$ simulations being somewhat smaller than
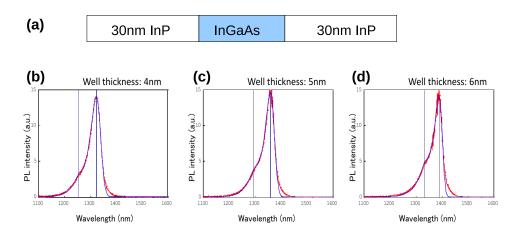
FIG. 4: (a) Illustration of the superlattice structure used for PL measurement. The barrier material InP is 30nm thick. (b)-(d) The PL measurement for 4nm $In_{0.53}Ga_{0.47}As$ (b), 5nm $In_{0.53}Ga_{0.47}As$ (c), and 6nm $In_{0.53}Ga_{0.47}As$ (d). The red curves are measurements, and blue curves are Gaussian fit. The first (lowest) peak values are summarized in Table II.

those reported in experiment; perhaps in the experiment the well widths are not absolutely controlled thus slightly smearing the gap towards bulk values.

IV. CONCLUSION

In this paper, we demonstrate that DFT calculations using DFT+U can be an efficient way to determine the band alignments between two alloys. The full procedure can be divided into two steps. The first step is to determine U values of a bulk alloy by automatically optimizing atomic orbital-specific values of U so that the experimental bandgap and the lattice constant agree with the values obtained in the simulation. The second step is to use these fitted U values in a superlattice calculation (with lattice relaxation), and the valence and conduction band offsets are then determined from the projected DOS away from the interface. We apply this procedure to InGaAs/InP, InGaAs/InAlAs, and InAlAs/InP, and are able to obtain both VBOs and CBOs consistent with experiments. The degree of non-transitivity ~ 0.1 eV in the calculated band alignments is in agreement with experiment. In addition the computed quantum-well width-dependent bandgaps of InGaAs/InP are in

good agreement with the photoluminescent measurements. The proposed method is semi-empirical, because optimization of U values requires knowledge of experimental bandgaps and lattice constants. However, it provides meaningful valence and conduction band offsets between two alloys, with the interface strain taken into account. For many semiconductor alloys the experimental data are available for at least 3 compositions, that is for $x = 1, 0$ and 0.5 in the $A_x B_{1-x} C$ alloy. Because empirical composition-bandgap dependencies (section II E) are quadratic, it seems plausible that the set of U values can be likewise interpolated by a quadratic polynomial. The use of a compact numerical atomic orbital basis sets as implemented in SIESTA package makes this method quite lightweight, amenable to large (300+ atoms) supercell computation on a single workstation. Because lattice relaxation is taken into account, the proposed procedure can serve as a practical method to explore the band alignments between complicated alloys.

Acknowledgement

---

[1] G. Yang, R. J. Hwu, Z. Xu, and X. Ma, IEEE Journal of Selected Topics in Quantum Electronics **6**, 577 (2000).

[2] Y. Chen, D. Radulescu, G. Wang, F. Najjar, and L. Eastman, IEEE electron device letters **9**, 1 (1988).

[3] J. P. C. Baena, L. Steier, W. Tress, M. Saliba, S. Neutzner, T. Matsui, F. Giordano, T. J. Jacobsson, A. R. S. Kandada, S. M. Zakeeruddin, et al., Energy Environ. Sci. **8**, 2928 (2015).

[4] D. O. Scanlon, C. W. Dunnill, J. Buckeridge, S. A. Shevlin, A. J. Logsdail, S. M. Woodley, C. R. A. Catlow, M. J. Powell, R. G. Palgrave, I. P. Parkin, et al., Nat. Mater. **12** (2013).

[5] Y.-H. Kuo, Y. K. Lee, Y. Ge, S. Ren, J. E. Roth, T. I. Kamins, D. A. B. Miller, and J. S. Harris, Nature **437** (2005).

[6] W. Kohn and L. J. Sham, Phys. Rev. **140**, A1133 (1965).

[7] M. Peressi, S. Baroni, A. Baldereschi, and R. Resta, Phys. Rev. B **41**, 12106 (1990).

[8] M. S. Hybertsen, Applied Physics Letters **58** (1991).

[9] C. G. Van de Walle and R. M. Martin, Phys. Rev. B **35**, 8154 (1987).

[10] S. Lany and A. Zunger, Phys. Rev. B **78**, 235104 (2008).

[11] L. Hedin, Phys. Rev. **139**, A796 (1965).

[12] X. Zhu and S. G. Louie, Phys. Rev. B **43**, 14142 (1991).

[13] J. P. Perdew, M. Ernzerhof, and K. Burke, J. Chem. Phys. **105** (1996).

[14] J. Heyd and G. E. Scuseria, J. Chem. Phys. **121**, 1187 (2004).

[15] V. I. Anisimov, J. Zaanen, and O. K. Andersen, Phys. Rev. B **44**, 943 (1991).

[16] S. L. Dudarev, G. A. Botton, S. Y. Savrasov, C. J. Humphreys, and A. P. Sutton, Phys. Rev. B **57**, 1505 (1998).

[17] S. Lany, H. Raebiger, and A. Zunger, Phys. Rev. B **77**, 241201 (2008).

[18] A. D. Becke and E. R. Johnson, The Journal of Chemical Physics **124**, 221101 (2006).

[19] A. D. Becke and M. R. Roussel, Phys. Rev. A: At., Mol., Opt. Phys. **39**, 3761 (1989).

[20] F. Tran and P. Blaha, Phys. Rev. Lett. **102**, 226401 (2009).

[21] D. Waroquiers, A. Lherbier, A. Miglio, M. Stankovski, S. Poncé, M. J. T. Oliveira, M. Giantom assi, G.-M. Rignanese, and X. Gonze, Phys. Rev. B **87**, 075121 (2013).

[22] S. V. Faleev, M. van Schilfgaarde, and T. Kotani, Phys. Rev. Lett. **93**, 126406 (2004).

[23] M. van Schilfgaarde, T. Kotani, and S. Faleev, Phys. Rev. Lett. **96**, 226402 (2006).

[24] A. N. Chantis, M. van Schilfgaarde, and T. Kotani, Phys. Rev. Lett. **96**, 086405 (2006).

[25] W. Kang and M. S. Hybertsen, Phys. Rev. B **82**, 085203 (2010).

[26] A. Wadehra, J. W. Nicklas, and J. W. Wilkins, Applied Physics Letters **97**, 092119 (2010).

[27] M. Gmitra and J. Fabian, Phys. Rev. B **94**, 165202 (2016).

[28] Y. Wang, F. Zahid, Y. Zhu, L. Liu, J. Wang, and H. Guo, Applied Physics Letters **102**, 132109 (2013).

[29] The transitivity rule refers to the following: for three semiconductors, A, B, and C, the band offset at the heterojunction A/B can be deduced from the band offsets at the heterojunctions A/C and C/B.

[30] J. M. Soler, E. Artacho, J. D. Gale, A. García, J. Junquera, P. Ordejón, and D. Sánchez-Portal, J. Phys.: Condens. Matter **14**, 2745 (2002).

[31] S. García-Gil, A. García, N. Lorente, and P. Ordejon, Phys. Rev. B **79**, 075441 (2009).

[32] J. P. Perdew, K. Burke, and M. Ernzerhof, Phys. Rev. Lett. **77**, 3865 (1996).

[33] A. I. Liechtenstein, V. I. Anisimov, and J. Zaanen, Phys. Rev. B **52**, R5467 (1995).

[34] M. Cococcioni and S. De Gironcoli, Phys. Rev. B **71**, 035105 (2005).

[35] V. Ivády, R. Armiento, K. Szász, E. Janzén, A. Gali, and I. A. Abrikosov, Phys. Rev. B **90**, 035146 (2014).

[36] F. Aryasetiawan, K. Karlsson, O. Jepsen, and U. Schönberger, Phys. Rev. B **74**, 125106 (2006).

[37] L. A. Agapito, S. Curtarolo, and M. B. Nardelli, Phys. Rev. X **5**, 011006 (2015).

[38] H. J. Kulik, N. Seelam, B. D. Mar, and T. J. Martínez, J. Phys. Chem. A **120**, 5939 (2016).

[39] P. Hohenberg and W. Kohn, Phys. Rev. **136**, B864 (1964).

[40] T. Kreibich, R. van Leeuwen, and E. K. U. Gross, Phys. Rev. A: At., Mol., Opt. Phys. **78**, 022501 (2008).

[41] H. Sonomura, G. Sunatori, and T. Miyauchi, Journal of Applied Physics **53**, 5336 (1982).

[42] R. E. Nahory, M. A. Pollack, W. D. J. Jr., and R. L. Barns, Applied Physics Letters **33**, 659 (1978).

[43] J. Minch, S. Park, T. Keating, and S. Chuang, IEEE Journal of Quantum Electronics **35** (1999).

[44] Y. Zhang, Y. Ning, L. Zhang, J. Zhang, J. Zhang, Z. Wang, J. Zhang, Y. Zeng, and L. Wang, Opt. Express **19**, 12569 (2011).

[45] D. Olego, T. Y. Chang, E. Silberg, E. A. Caridi, and A. Pinczuk, Applied Physics Letters **41**, 476 (1982).

[46] I. Vurgaftman, J. Meyer, and L. Ram-Mohan, Journal of applied physics **89**, 5815 (2001).

[47] S. Adachi, P. Capper, S. Kasap, and A. Willoughby, *Properties of Semiconductor Alloys: Group-IV, III-V and II-VI Semiconductors*, Wiley Series in Materials for Electronic & Optoelectronic Applications (Wiley, 2009), ISBN 9780470743690.